INVESTIGATION OF THE AERODYNAMIC CHARACTERISTIC OF SOLAR POWERED LAWN MOWER BLADES

Manuscript Info

Manuscript History
Received: xxxxxxxxxxxxxxx
Final Accepted: xxxxxxxxxxx
Published: xxxxxxxxxxxxxxx

Key words: -
Computational fluid dynamics, Nodal stress analysis, Pollution control, Principalcomponentanalysis, Solar energy, Spiral blades.

Abstract

Gasoline lawn mowers release a significant amount of pollutants into the atmosphere, making them a contributor to environmental degradation. To address this issue, the focus shifts to enhance the cutting performance of manual lawn mowers powered by solar energy. Through careful design and fabrication, solar lawn mowers are developed to evaluate their effective field capacity, which refers to the area that can be effectively mowed within a specific period. In addition to assessing field capacity, a stress analysis of the mower blades is carried out to identify the most suitable materials and conditioning processes that will optimize their performance during operation. The investigation not only explores mechanical aspects but also delves into the aerodynamic properties of the blades, particularly those shaped like the NACA5616 airfoil, which is installed on the lawn mower. The aerodynamic analysis focuses on understanding the lift-drag performance of the airfoil section when exposed to airflow in a typical mowing scenario. The results are quantified through detailed C_L (coefficient of lift) and C_d (coefficient of drag) graphs, which depict the relationship between these two critical factors. Validation of these graphs ensures accuracy in the findings and underscores the effectiveness of the airfoil design. Moreover, the study visualizes the velocity contours around the blade at several angles—specifically 30, 60, and 90 degrees. This visualization is crucial for analyzing the vortex and wake effects that develop as the blade moves through the air. By examining these effects, insights are gained into how the design of the blades impacts performance, allowing for further optimizations to enhance both efficiency and effectiveness in lawn maintenance with reduced environmental impact. Overall, the findings demonstrate a statistically significant improvement in the lift-to-drag ratio, indicating that the aerodynamic design can lead to better performance in solar-powered mowing applications.

Introduction: -

Lawn care is a crucial aspect in maintaining the aesthetic appearance of residential and commercial properties. The agricultural industry, along with its associated sectors, constitutes 52 percent of the total labour force in India [1].Historically, gasoline-powered lawn mowers have been the primary tool used for mowing grass.However, with growing concerns about air pollution and environmental sustainability, there has been a shift towards the use of solar-powered lawn mowers. The first grass cutting machine was conceived by Edwin Beard, and it had a gear system coupled with a big roller and cutting cylinder [2].We would like to discuss some of the recent development in the technology of lawn mowing. *Pirchio et.al.* (2018) examined the efficacy of autonomous mowing in controlling the growth of creeping weeds. Although their findings suggest that this method may not be highly efficient in preventing weed proliferation, it does have several advantages in other domains. For instance, the use of autonomous mowing technology has been associated with enhanced turf quality and decreased resource consumption [3].Consequently, the advancement of lawn cutters strongly relies on the progress made in this field. According to the findings of *Sivagurunathan et.al;(2017),* a significant majority of homeowners in Malaysia, specifically seventy percent, opt for gas-powered lawn mowers when engaging in their routine grass mowing activities [4].

1.1. Recent advancement in the development of Lawn mower

Emissions from vehicles and conventional lawnmowers have the potential to generate higher levels of volatile organic compounds (VOCs) in the atmosphere as stated by *Batterman et.al.(2006). Liao et.al., (2021)* investigated the utilization of Raspberry Pi for image recognition and the development of human-machine interface for an automatic lawn mower. The core controller for this system is TMS320F2808, a digital signal processor (DSP)chip [5].*Satwik et.al.,(2015)* conducted a study wherein they explored the design and production of a lever operated solar lawn mower. In addition, they conducted contact stress analyses on spur gears and the objective was to develop a mechanism that enables the adjustment of the cutting blade's height [6].According to an investigation conducted by *Priest et.al.,(2000)* lawnmowers are responsible for 5.2 and 11.6% of Carbon monoxide (CO) and Non-Methane Hydrocarbon (NMHC) emissions respectively in the Newcastle research region [7]. *Derander, et al., (2018)* designed a smart robot lawn mower that can function without a boundary cable [8]. *Ahmad et.al.,(2016)* developed a lawn mower robot that has the ability to avoid obstacles using an ultrasonic sensor by (FPGA) programming that is used to control the movements and all data and information are processed [9]. Lawn mower's autonomous coverage of a specified area and manual control via RC transmitter are possible as stated by *Aponte et.al.,(2019)* in which (VHSIC) hardware description language (VHDL) is used to describe the hardware using Quartus II software [10].

Ibrahim et.al.,(2020) [11] designed an autonomous remote monitored solar lawn mower to monitor, control, and give information to the user. *Lerman et.al.,(2019)* [12]investigated the mixed effects modelling approach which was employed to examine the interaction between variables and their response to varying mowing frequencies and found that the frequency at which lawns were mowed did not have a significant impact on soil temperature, moisture levels, or the fluxes of biogenic soil.Autonomous mowers were projected to use about 4.80 kilowatt hours per week, whereas gasoline-powered rotary mowers used about 12.60 kilowatt hours per week as stated by *Grossi et.al* [13].*Galceran & Carreras,(2013)* [14] discussed about coverage path planning (CPP), a process for identifying a trajectory that encompasses all the specified points within a given area or volume of interest, while simultaneously avoiding any potential obstacles that may be present. This particular task holds significant importance in various robotic applications, including in creating image, autonomous vehicle, and grass cutters.The STC algorithm for lawn mowing was improved by *(Weiss et.al.,2008)* [15]through the optimization of U-turns along with the path and the introduction of the ability to shift the mowing direction. Exhaust emissions from standard lawnmowers contain measurable amounts of carbon monoxide, hydrocarbons, nitrogen oxides, particulate matter, polycyclic aromatic hydrocarbons, methane, ethane, and ethene, ethanol, and nitrous oxide examined by *Christensen et.al.,(2001)* [16]. In a field test conducted by *Priest et.al.,(2000)* with 19 two stroke and 10 four stroke lawn-mowers operated with oil and gas contribute 5.2 and 11.6% of CO and NMHC emissions.The utilization of a mobile phone as a mean of controlling a node MCU ESP8266 as studied by *Liao et.al.,(2021)* which has been pre-programmed to assume command over specified input and output functions, is observed and the motor driver is responsible for controlling the DC motor to facilitate its movement and the mobile phone is positioned in a higher position relative to the lawnmower, enabling it to transmit the electrical pathway and execute the task of cutting the grass[5].

1.2. Problem Origin and Novelty of the Statement

The conventional gasoline-powered lawn mower is characterized by a comparatively high fuel consumption rate, which correlates with moderate efficiency levels in its operation. In the pursuit of better performance, researchers have explored various enhancements by integrating advanced processors and electronic components into the design of the lawn mower. Despite these efforts, there exists a significant opportunity for performance improvement through modifications to the mower's blade profile. In the recent study, the conventional linear blade of the lawn mower has been replaced with a curved helical design. This innovative blade configuration originates from the central axis of the mower and features a curved section at the forefront that resembles a cutout portion of an airfoil. This design aims to optimize the harvesting of solar energy by effectively capturing sunlight through the installation of solar panels on the mower. Traditionally, the implementation of a complete airfoil at the leading edge of the blade has not been favored due to concerns about increased weight and potential balancing difficulties that may arise from such modifications. However, the current design approach utilizes a conventional lawn mower as the foundational model, upon which these innovations are built. To assess the efficacy of the newly designed blade system, a computational simulation was conducted using ANSYS Fluent, a sophisticated computational fluid dynamics (CFD) software. This simulation specifically focused on the performance of the cutting blades under different operational conditions. The reliability and accuracy of the simulation results were corroborated by comparing them with data previously reported in scientific literature.

2.Methodology

The panels of a solar grass cutter are arranged in a certain way so that they may absorb the maximum amount of direct sunlight possible. The Solar panels collect light from the sun and convert it into usable electricity. A solar charger is utilized to capture solar energy and subsequently store it in the rechargeable batteries. The blades on a lawn mower are the most crucial component because they determine how well the grass is cut. Depending on their intended function, lawn mower blades can be categorized as either straight, low-lift, high-lift, mulching, or gator. The solar-powered lawnmower is comprised of several essential components, namely a direct current motor, a rechargeable battery, a solar panel, a blade made of stainless steel, and a control switch.

2.1. Geometric Details.

The DC motor generates the necessary torque to propel the stainless-steel blade, which is directly connected to the shaft of the DC motor, thereby enabling efficient mowing. The switch on the board shuts the circuit, allowing electricity to flow to the motor, which spins the blade of the solar-powered lawnmower. The solar charging controller is responsible for recharging the battery.

The effectiveness of the new equipment was tested on a variety of grasses. The operational site for lawn mowing activities is situated at the coordinates 26°33′ N and 91°43′ E, specifically located within Kamrup polytechnic in the state of Assam. A pyranometer and a stopwatch were employed to quantify radiation levels and record time over a period of three consecutive days. Material of the handle is made from aluminum and polyester material is used. (Table 1) show the standard dimensions for a solar-powered lawn mower.

Table 1. Lawn mower geometry parameters

Number	Parameter	Value	Dimension
1	Dimension of Solar lawn setup	49x35x81	mm
2	Shaft diameter (d_{sh})	5	mm
3	Blade thickness (t_b)	0.5	mm
4	Blade diameter (dl_b)	240	mm
5	Wheel diameter (dl_ω)	90	mm

3.Result and Discussion.

Before the fabrication, development, and manufacture of the lawn cutting blade, the design of the blade is carried out on SolidWorks. After that, a computational fluid dynamics (CFD) analysis of the blade is carried out at Ansys 2018R2 to calculate the blade's torque and power. The geometric dimensions of the computational model were consistent with those of the experimental model.

The distribution of local forces along the blade's edge varies as the curvature changes and the optimization of the variable "n" is examined in conjunction with considerations regarding the presence or absence of constraints on the material to be trimmed, the investigation also explores the mechanics involved in the process of cutting by a cylinder lawn mower *Atkins,(2006)[17]*.

3.1. Numerical Simulation and Computational Domain

In order to establish the fluid-structure interaction surface in the coupling, a very tiny thickness is assumed in the simulation. It has generally a fixed blade and hub. It has all major parts fixed relative to the main shaft. The hub should be able to bear all the high loads on shafts and bending moment at blade roots. This will also include the aerodynamic loads on the blades and dynamic induced load due to blade rotation and yawning motion. Using Ansys workbench and the moving meshing approach, a numerical simulation is done to analyse the blades' motion and estimate their performance.

(Table 2) displays the principal simulation parameters. Due to system coupling, the interaction force between the fluid and the solid portions must be communicated across the fluid-structure interaction surface during the fluid-structure interaction process. Circular and rectangular boundaries are defined within the computational domain to enclose the blade. Grids are then generated within these boundaries.

A rectangular enclosure is utilized to examine the fluid dynamics surrounding the blade. The boundaries of the enclosure are intentionally placed at an appropriate distance to the blade in order to prevent any interference with the results that are being obtained. On the contrary, a circular boundary is created in the vicinity of the blade region in order to meticulously assess the mesh and investigate the impact of nearby mesh on the performance of the rotating blade. The resolution of the boundary layer in close proximity to the walls allows for thorough monitoring of the impact of the shear zone on the performance of the blade.

Table 2. Moment simulation parameters

Moments (0 0 0)				Moment axis (0 0 1)		
	Moment (Nm)			Coefficients		
Blade	Pressure	Viscous	Total	Pressure	Viscous	Total

Net	1.339	-0.074	1.324	228.45	-12.39	216.213

3.2. Meshing

An hexagonal prism grids of 1350783 being used to mesh the flow domain (Fig. 2). It is to the cutting advantage that the blade was designed with a minute curve running down its edge, as this makes for a smoother flow of air when the blade is in action *Arunkumar et.al.,(2021)[18]*. A 2d blade profile is plotted (Fig 3) from the Q blade software. The current investigation is for the airfoil configuration of NACA 5616.The suction of the soil pulls the grass up, making for an easy cut. In contrast, the vertical edges of a straight blade provide almost minimal suction. This causes a tiny amount of air to be forced over the blade. In order to facilitate the advancement of blade design and computation, it is imperative to ascertain the minimum cutting force of a blade. High pitch is provided to the root side, which results in high velocity being generated at the tip, which also shows that the angle at the root is less than the angle at the tip.

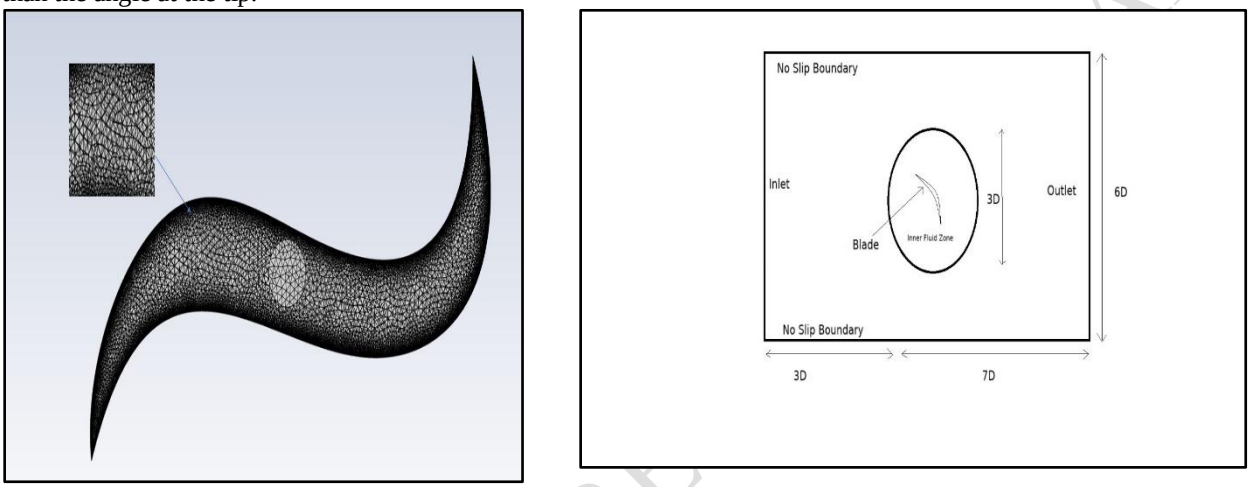

Fig. 2. Hexagonal mesh structure (left side) and computational model of blade in full domain (right side).

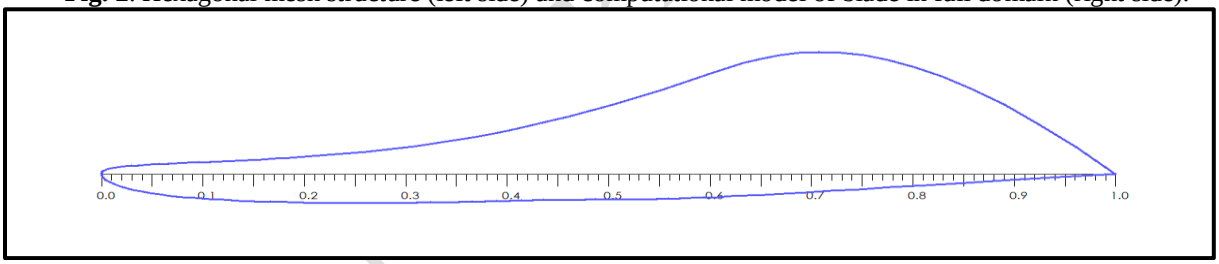

Fig.3.NACA 5616 profile

3.3 Computational analysis of the blade

Each successive layer in the inflate zone has expanded with 1.2 up to the fifth layer, with the initial rise of the grid lines from the blade surface being 0.02 mm. The present research considers a number of boundary conditions, including a velocity entry in the left boundaries of the field, domain outflow condition, wall condition, treating the interior fluid as the interior, treating the exterior fluid as the exterior, and slip conditions on the side boundaries. These boundary conditions are detailed in (Table 3). The parameters for NACA 5616 are m=0.052c, t=0.167c and p=0.67c where m is the maximum camber, t is the thickness and p are the position of the camber.

Table 3. Boundary condition used for the solar lawn mower blade.

Sl. No	Zone	Type
1	Inlet	Velocity inlet
2	outlet	outflow
3	Interior fluid	interior
4	Outer fluid	exterior
5	blade	Moving wall
6	wall	No slip boundary

The computational condition for evaluating the cutting blade involves conducting tests using air as the medium. The air has a density of approximately 1.29 kg/m^3 and a viscosity of 0.000016 kg/m-s. The velocity of the air is maintained at a range of 4-5 m/s. The computational model employed in this study is the shear stress transport (SST) k-w model, while the computational fluid dynamics (CFD) algorithm utilized is the semi-implicit method for pressure-linked equations (SIMPLE) with a second-order upwind interpolation scheme. The near wall treatment is maintained under standard conditions. The computational domain is discretized by the ANSYS Design modeler into finite control volumes.

The Fluent CFD solver then integrates the transportation variables of the continuation and navier-Stokes equations onto these control volumes. The procedure produces a collection of governing equations expressed as algebraic equations. The equations are subsequently solved iteratively, considering the specified boundary conditions. The Semi-Implicit Pressure Linked Equations (SIMPLE) an algorithm is employed to effectively integrate the pressure and velocity terms within the pressure correction equation. During the spatial discretization phase of the simulation, the least square cell-based gradient technique is utilized to enforce the terms of the equations that govern the simulation.

The lift and drag coefficients are determined through computational simulations conducted at distinct positions for each airfoil and these positions correspond to varying angles of attack (AoA) ranging from -15 to 25 degrees and these low angles of attack are typical for the operation of tip airfoil as investigated by *Papi et.al.,(2021)[19]*. The distribution of roughness on an airfoil has the effect of increasing turbulent fluctuations within the boundary layer, thereby promoting early transition as stated by *Feindt,(1957) Yang & Xiao,(2019) Munduate & Ferrer,(2009*)[20-22].The blade relative velocity is calculated by taking the vector sum of the absolute wind velocity U and the reciprocal of the blade tangential speed.

At the blade position, the blade's location is determined by the coordinates of its centre of pressure investigated by *Castelli et.al.,(2011)[20]*. The turbine rotor blade as investigated by *Howell et.al.,(2010)* with its characteristic 4:1 aspect ratio, spins at low tip speeds, also its performance exhibits a discernible correlation with the surface finish of the rotor blade. The imaginary component is responsible for determining the aeroelastic stability of the rotor. In the event that mechanical damping is not present, the stability of the rotor is contingent upon the condition that the imaginary moment remains negative for all inter blade phase angles investigated by *Hall et.al.,(2002)[21]*.The values of the lift- drag coefficients have reached convergence at the 106^{th} iteration. The validation of graph between coefficient of lift and geometric angle of attack depicting the airfoil simulation of NACA 5616 (Fig 4) and compared it with the *(Kozak, 2014)[23]* model and the experimental graph by *Piziali,(1994)[22]*. Additionally, the graph assessed against the ideal lift curve. The observed phenomenon indicates that there is a positive correlation between the angles and the speeds, which is in line with the displacement of the curves observed with the elevation of the Reynolds numbers. The coefficients were computed utilising the least square technique, which involved fitting the empirical data obtained from the NACA 5616 airfoil at a Reynolds number of 10^6.(Fig.5) represent the graph for coefficient of lift and drag. The polar angle was fixed at minimum -15º to 25º maximum for this blade profile. Similarly, validation of the graph in (Fig.6) between drag coefficient and geometric angle of attack depicting the airfoil simulation of NACA 5616 by comparing it with the Kozak model and the experimental model by Piziali.

3.4 Static Nodal stress analysis of the blade

During the initial computational step, the centrifugal load is incrementally applied, starting from a stationary state and gradually increasing until it reaches the nominal speed. During each computational iteration of the centrifugal step, a nonlinear static analysis is conducted to examine the stiffening effect and the slipping contact condition *Szwedowicz, et.al.,(2005)[24]***.** The finite element can be employed for blade impact research in a number of different numerical approaches *Huang and Liaw,(2001)[25]*. Study conducted by *Simo,et.al.,(1986)[26]* compared the perturbed and augmented approaches. The Lagrange multiplier method *Nour and Wriggers,(1986)* [27]and the penalty method *Auricchio, (1996)[28]* have seen similar application.

Table 4. Mechanical properties of the material

Sl. No	Properties	Plain Carbon steel	1060 Al alloy	Alloy steel
1	Density	7.8 g/cc	2.7 g/cc	7.7 g/cc
2	UTS	685 Mpa	110 Mpa	650Mpa
3	Poisson's ratio	0.28	0.33	0.28
4	Modulus of elasticity	207 Gpa	70 Gpa	200Gpa
5	Tensile Strength	399.82 Mpa	62 Mpa	620.42 Mpa
6	Deformation Scale at Pressure of 1Mpa	0.002613	0.000863	0.002623

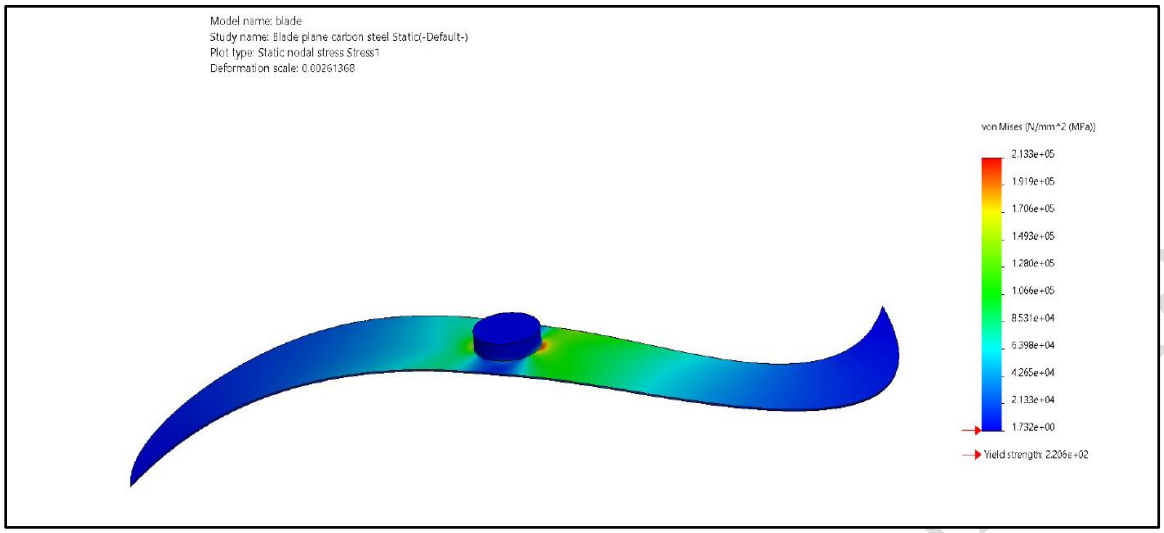

Fig.7. Static stress plot of plain carbon steel blade

Because the von mises stress is higher than the material's yield limit, it is possible to draw the conclusion that the material will yield rather than fracture based on a deformation scale of 0.0026 in plain carbon steel. This is since the yield limit of the material is lower than the von mises stress. 1 MPa was the value of the pressure that was delivered to the faces of the blade. The element growth size ratio of 1.4 was utilised in the creation of a fine blended curvature mesh. Table 4 shows the results of a deformation scale derived from solid works, from which 1060 alloy steel undergoes less deformation than the other two materials.

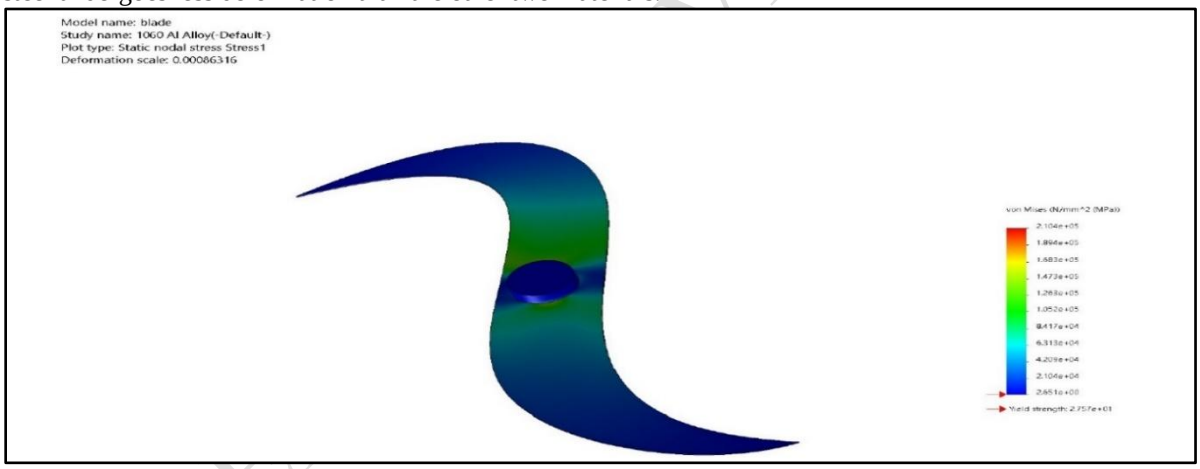

Fig.8. Static stress plot of 1060 aluminum alloy

When the shaft is not moving, it is vital to remember that the curved blades do bend because of gravity. However, once the shaft begins to rotate, the centrifugal forces of the blades, which are proportional to the speed of rotation, finally overcome the bending strains. *Tiju et.al.,(2015) [29]*. The quantity of blades has a notable impact on the overall torque, resulting in a reduced fluctuation in instantaneous shaft torque when more blades are present. (Fig.7,8 and 9) illustrates the stress analysis conducted on different materials, namely carbon blade, aluminum alloy, and alloy steel, all of which are potential options for blade applications.

It is evident that a mower featuring only one blade is not a viable option from a technical standpoint. This is due to the significant balancing issue it poses, necessitating the use of a counterweight to ensure proper operation. Additionally, the presence of a counterweight would increase parasitic drag, further complicating the blades functionality *Paraschivoiu,(2022)[30]*.The blade design affected the amount of force needed to cut stems/grass, and a 26% difference was noted between the test designs *Clementson and Hansen,(2010)[31]*.

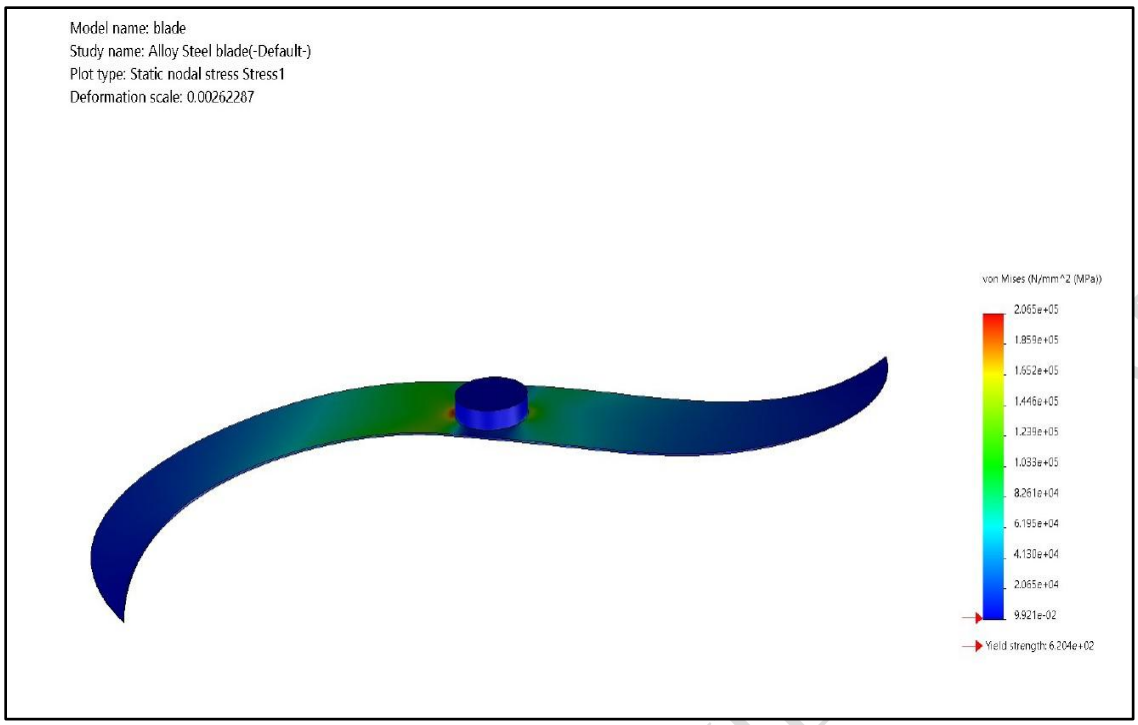

Fig. 9. Static stress plot of alloy steel blade

A small number of blades, like two or three, seems to be the best option. Adding a third blade would decrease the torque ripple, but it would also raise the cost of the mower and, in the end, the system's cost of energy (COE).

3.5 Study of velocity contours in the blade

(Fig. 10.1 to Fig 10.6) represent the various velocity contours at various angles and at different rotational speed of the blade varying from 100 rpm to 500 rpm. The maximum wake effect in the blade can be seen at higher rotational speed that is ranging at 500 rpm. (Fig. 10.5) represent the maximum wake effect at higher angle and lower rpm. The blades were positioned at different angles and analysis were performed on different velocities of blade. From (Fig. 10.5 and 10.6) the velocity contour demonstrates that a large wake is produced at high rotational angles and stabilized at higher speed, and that this wake decreases as rotational speed decreases. Less wake is produced in the modular stack blade because of the bigger pressure difference in the blade as investigated by *Bedon, et al.,(2015)[32]*. Low speed to high-speed vectors were observed in 400 rpm.

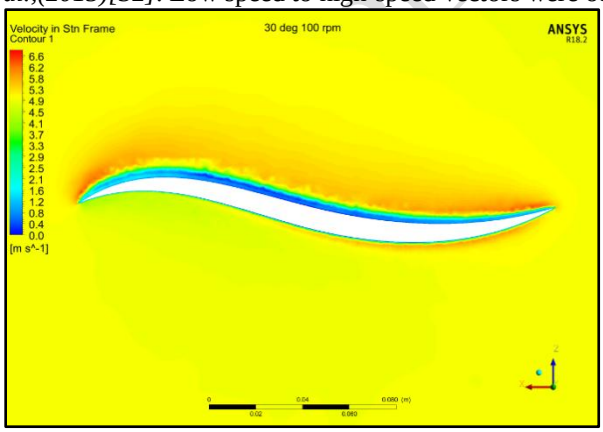

Fig. 10.(a). Velocity Contour of blade at 30º with a rotational speed of 100 rpm.

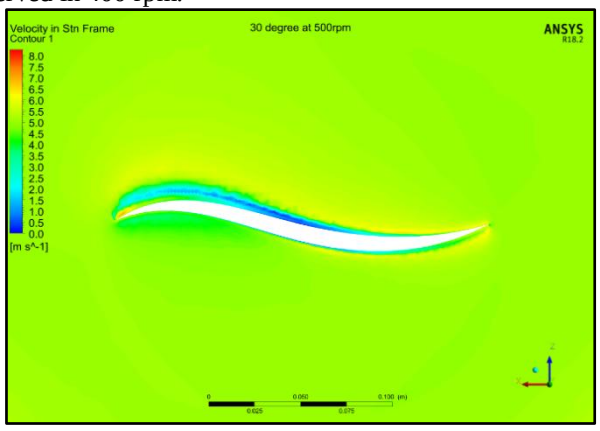

Fig. 10. (b). Velocity Contour of blade at 30º with a rotational speed of 500 rpm.

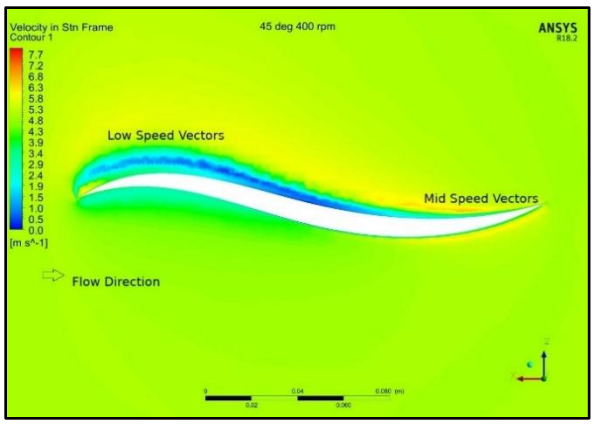

Fig. 10. (c). Velocity Contour of blade at 45º with a rotational speed of 400 rpm.

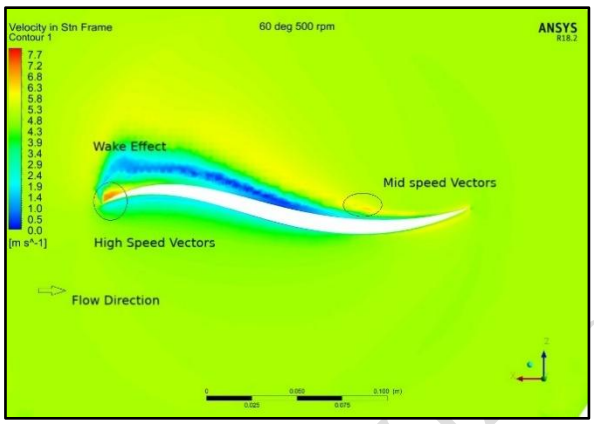

Fig. 10. (d). Velocity Contour of blade at 60º with a rotational speed of 500 rpm.

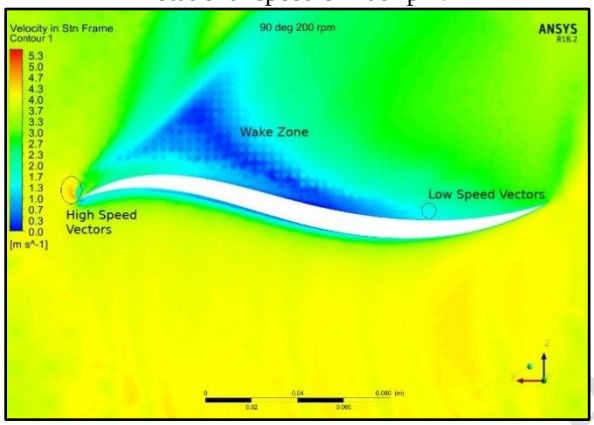

Fig. 10. (e). Velocity Contour of blade at 90° with a rotational speed of 200 rpm.

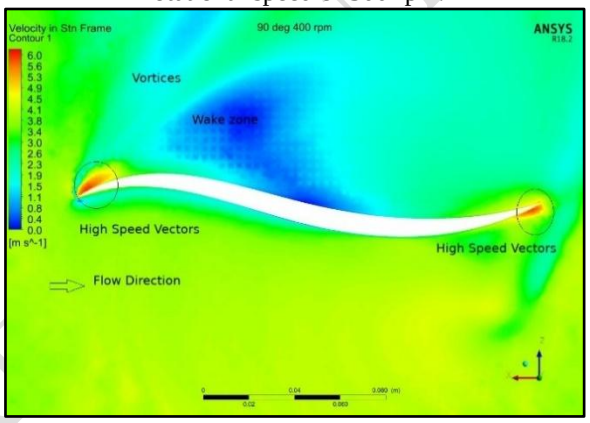

Fig. 10. (f). Velocity Contour of blade at 90° with a rotational speed of 400 rpm.

The peak wake impact on the blade is observable at elevated rotational velocities, specifically within the range of 500 revolutions per minute. The incorporation of external dimples on the upper surface of an aerofoil leads to an enhancement in its aerodynamic capabilities. The incorporation of circular dimples on the upper surface has resulted in the generation of a high velocity region in the proximity of said surface, in contrast to the regular surface model. The blade profile with dimples on its upper surface has exhibited a higher lift to drag ratio in comparison to the regular surface aerofoil. Wake effect maximizes at 90º with a rotational speed of 200 rpm and 400rpm.

Solar-powered lawn mowers could incorporate enhancements in solar panel technology, resulting in increased energy conversion rates and enhanced efficiency. This would enhance operational duration and optimize solar power utilization. The research gap in the incorporation of smart and autonomous technologies can improve the performance of solar-powered lawn mowers. Autonomous mowers may incorporate artificial intelligence (AI) and sensors to efficiently maneuver lawns, identify barriers, and optimize mowing techniques. GPS technology may be integrated into the equipment to facilitate accurate and effective mowing. The development of mower primary emphasis is placed on the user experience, encompassing level of ease in utilizing the product, the extent of maintenance needed, the degree of noise generated, and the overall level of user contentment.

Estimation of effective field capacity using principal component analysis.

Principal component analysis (PCA) is a method used to analyse a dataset that consists of multiple quantitative dependent variables that are inter-correlated as defined by *Abdi and Williams,(2010[33]*. In this section, we begin by providing the theoretical background for two variations of a technique known as multiple regression. Specifically, we examine the application of multiple regression using both manifest variables and their principal components. Our aim is to establish the fundamental concepts and notation necessary to explore the relationships between blade cutting speed, time for cutting grass, effective field capacity and efficiency.

PCA is employed to identify the degree of correlation among these parameters, particularly in relation to cutting blades. To derive a more significant representation of the dataset, it is crucial to streamline the number of factors down to a manageable number of linear permutations of the data. A principal component will be assigned to

each linear combination. The results of the principal component analysis (PCA) conducted on the correlation matrix indicate the presence of two principal components *Abdelhafidi,et.al.,(2021)[34]*.These components have eigenvalues exceeding 1.00, indicating their significance in explaining the variance in the data. Collectively, these two components account for 88.59% of the total variance observed in the dataset. The size of their eigenvalues establishes the relative significance of these variables, as shown in (Table 5).

Table 5. Principal component for effective field capacity.

PCs	Eigenvalues	Variance (%)	Cumulative Variance
PC1	3.276	54.62	54.62
PC2	2.038	33.97	88.59

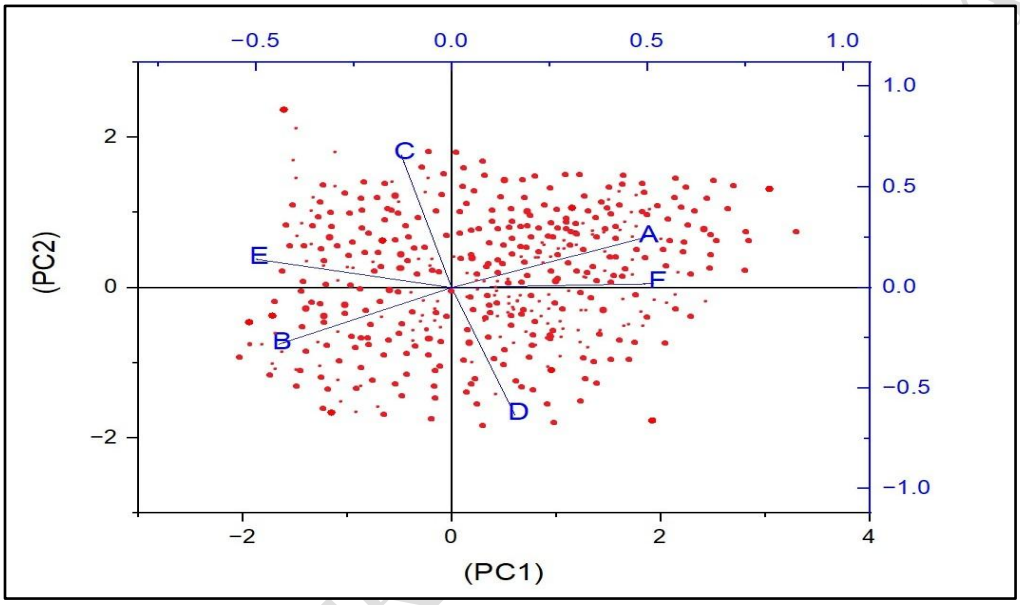

Fig.11.Variables contribute, with the length of the vectors reflecting their relative importance to the principal components and the angle between any two components reflecting the degree of their association.

For each PCA, we chose as representative variables three different components with factor loadings over 0.43 to identify the most important variables for subsequent regression analysis. In this study, a threshold value of 0.43 was employed to determine the presence of a dependable factor (Table 6). Hence, the initial principal component exhibits a significant correlation with four of the original variables, displaying an upward trend as the duration of sunshine increases. This implies that there is a correlation between these criteria. If the value of one variable increases, it is likely that the values of the remaining variables will also increase. The component also exhibits an increase as cloud cover decreases particularly in forenoon.

Table 6. Outcomes of the principal component analysis are presented in the component matrix. (Bold values represent highly corelated PC variables, FD refers to forenoon day and AD refers to afternoon day).

Variables	**Principal component**	
	PC1	*PC2*
FD 1	**0.4944**	**0.2497**
AD 1	-0.4420	-0.2821
FD 2	-0.1290	**0.6610**
AD 2	0.1617	-0.6631
FD 3	-0.4997	0.1408
AD 3	**0.5173**	0.0190

The relationship between the second principal component and cutting speed is positive, indicating that as cutting speed increases, the second principal component also increases**.** (Fig. 11) clearly depicts the projections of variables using the principal components. In relation to the acquired outcome, there exists a single predictor variable, namely sunshine hours. This necessitates the implementation of stepwise multiple regression, wherein

variables are introduced incrementally. With this method, we may evaluate the existing explanatory variables for significance before adding any new ones to the equation. The variables that do not make a significant contribution are removed.

Table 7. Results from a three days multiple regression analysis that was performed in steps are shown. The root mean squared error (RMSE), coefficient of determination (R^2), probability value is reported.

Estimated Coefficient				**Regression Values**		
Estimate	Standard Error	t-stat	p value	RMSE	R^2	R^2 adj
Day 1 Number of observations =250, error degree of freedom=243						
0.00206	0.0015	14.26	0	0.94	0.89	0.88
Day 2 Number of observations =250, error degree of freedom=241						
0.00324	0.0028	11.18	0	0.91	0.82	0.79
Day 3 Number of observations =250, error degree of freedom=238						
0.00493	0.0031	15.77	0	0.95	0.91	0.90

The proposed model is grounded in two key meteorological input factors, which play a crucial role in its predictive capabilities. The model's performance is quantified by root mean square errors (RMSEs) of 0.94, 0.91, and 0.95, corresponding to three consecutive days of analysis. Additionally, the coefficient of determination, or R-squared values, for these days are reported at 0.89, 0.82, and 0.91, respectively. These metrics indicate the degree to which the model's predictions align with the observed data, with R-squared values approaching 1 indicating a strong correlation. The variations in sunshine hours over the three days significantly influence the effectiveness of the model, suggesting that sunlight exposure is an important factor in the overall prediction process. The model's ability to account for differing sunshine conditions enhances its accuracy and reliability in forecasting outcomes. Moreover, the concept of effective field capacities is introduced as an essential consideration in the context of lawn maintenance. The capacity for land to support various activities, particularly the cutting of grass at different heights, is intertwined with the meteorological variables utilized in the model. The implications of this are significant; with a well-established overall correlation, the model presents a viable tool for predicting the optimal conditions for grass cutting, accommodating for variations in grass height. This predictive accuracy positions the model as a recommended solution for practical applications in lawn care management. Table 7 illustrates the data supporting these findings, providing a visual reference for the changes in sunshine hours and their relationship to the model's performance metrics.

4.Conclusion

The study focuses on evaluating the lift and drag performance characteristics of NACA5616 models when tested under regular surface conditions. The testing involved a range of rotational speeds, specifically between 100 to 500 revolutions per minute (rpm). Notably, while the lift performance shows improvement with increasing rotational speed, there is a significant trade-off, as the coefficient of drag also rises in conjunction with higher angles of attack. In addition, the paper introduces a novel statistical methodology aimed at modeling global solar radiation, which is crucial for understanding the potential applications of solar energy in various contexts. Through this research, the authors seek to stimulate further exploration into numerical methods capable of addressing challenges associated with solar-powered lawn mowers. Identifying optimal climatic conditions plays a critical role in developing innovative designs for such equipment. Currently, there is a noticeable gap in the existing literature related to computational analyses of the blades used in solar lawn mowers. As a result, the findings from this study have not been thoroughly validated against practical outcomes, which limits their reliability. By applying effective optimization techniques tailored for blade design, there exists the potential for producing solar-powered lawn mowers that are not only efficient but also align with sustainability goals. This advancement can lead to enhanced performance and broader adoption of solar energy solutions in landscaping equipment.

Declaration of competing interest

The authors declare that they have no known financial or non-financial competing interests in any material discussed in this paper.

Funding information

No funding was received from any financial organization to conduct this research.

References

1.Fan, S., & Pandya-Lorch, R. (Eds.). (2012). Reshaping agriculture for nutrition and health. Intl Food Policy Res Inst.

2.A. Shukritis, "History of Lawn mowers," 2012.

3.Pirchio, M., Fontanelli, M., Frasconi, C., Martelloni, L., Raffaelli, M., Peruzzi, A., ... & Grossi, N. (2018). Autonomous mower vs. rotary mower: Effects on turf quality and weed control in tall fescue lawn. Agronomy, 8(2), 15.

4.Sivagurunathan, R. Linkesvaran and J. c. Jun Hao, "Design and fabrication of low cost portable lawn mower," scholars journal of engineering and Technology, vol. 10, no. 5, pp. 584-591, 2017.

5.Liao, J. C., Chen, S. H., Zhuang, Z. Y., Wu, B. W., & Chen, Y. J. (2021). Designing and manufacturing of automatic robotic lawn mower. Processes, 9(2), 358.

6.Satwik, D., Rao, N. R., & Reddy, G. S. (2015). Design and Fabrication of lever operated solar lawn mower and contact stress analysis of spur gears. International Journal of Science, 4(8), 2815-2821.

7.Priest, M. W., Williams, D. J., & Bridgman, H. A. (2000). Emissions from in-use lawn-mowers in Australia. Atmospheric Environment, 34(4), 657-664.

8.Derander, J. M., Andersson, P., Wennerberg, E., Nitsche, A., Moen, E., & Labe, F. (2018). Smart robot lawn mower. Department of Computer Science and Engineering Chalmers University of Technology University of Gothenburg Gothenburg, Sweden.

9.Ahmad, N., bin Lokman, N., & Abd Wahab, M. H. (2016, November). Autonomous Lawnmower using FPGA implementation. In IOP Conference Series: Materials Science and Engineering (Vol. 160, No. 1, p. 012112). IOP Publishing.

10.Aponte-Roa, D. A., Collazo, X., Goenaga, M., Espinoza, A. A., & Vazquez, K. (2019, January). Development and evaluation of a remote controlled electric lawn mower. In 2019 IEEE 9th Annual Computing and Communication Workshop and Conference (CCWC) (pp. 1-5). IEEE.

11.Ibrahim, B., Brahmaiah, V. S., & Sharma, P. (2020). Design of smart autonomous remote monitored solar powered lawnmower robot. Materials Today: Proceedings, 28, 2338-2344.

12.Lerman, S. B., & Contosta, A. R. (2019). Lawn mowing frequency and its effects on biogenic and anthropogenic carbon dioxide emissions. Landscape and Urban Planning, 182, 114-123.

13.Grossi, N., Fontanelli, M., Garramone, E., Peruzzi, A., Raffaelli, M., Pirchio, M., ... & Volterrani, M. (2016). Autonomous mower saves energy and improves quality of tall fescue lawn. HortTechnology, 26(6), 825-830.

14.Galceran, E., & Carreras, M. (2013). A survey on coverage path planning for robotics. Robotics and Autonomous systems, 61(12), 1258-1276.

15.Weiss-Cohen, M., Sirotin, I., & Rave, E. (2008, December). Lawn mowing system for known areas. In 2008 international conference on computational intelligence for modelling control & automation (pp. 539-544). IEEE.

16.Christensen, A., Westerholm, R., & Almén, J. (2001). Measurement of regulated and unregulated exhaust emissions from a lawn mower with and without an oxidizing catalyst: a comparison of two different fuels. Environmental science & technology, 35(11), 2166-2170.

17.Atkins, T. (2006). Optimum blade configurations for the cutting of soft solids. Engineering Fracture Mechanics, 73(16), 2523-2531.

18.Arunkumar, P. M., Muthu, N., Prathuman, V. G., Ukkashi, A. S., & Achuthan, P. V. (2021, March). Simultaneous Localization and Mapping Technique Based Autonomous Lawn Mower. In 2021 7th International Conference on Advanced Computing and Communication Systems (ICACCS) (Vol. 1, pp. 767-771). IEEE.

19.Papi, F., Balduzzi, F., Ferrara, G., & Bianchini, A. (2021). Uncertainty quantification on the effects of rain-induced erosion on annual energy production and performance of a Multi-MW wind turbine. Renewable Energy, 165, 701-715.

20.Castelli, M. R., Englaro, A., & Benini, E. (2011). The Darrieus wind turbine: Proposal for a new performance prediction model based on CFD. Energy, 36(8), 4919-4934.

21.Hall, K. C., Thomas, J. P., & Clark, W. S. (2002). Computation of unsteady nonlinear flows in cascades using a harmonic balance technique. AIAA journal, 40(5), 879-886.

22.Piziali, R. A. (1994). 2-D and 3-D oscillating wing aerodynamics for a range of angles of attack including stall (No. NASA-TM-4632).

23.Kozak, P. (2014). Effects of unsteady aerodynamics on vertical-axis wind turbine performance (Doctoral dissertation, Illinois Institute of Technology).

24.Szwedowicz, J., Slowik, S., Mahler, A., & Hulme, C. J. (2005, January). Nonlinear dynamic analyses of a gas turbine blade for attainment of reliable shroud coupling. In Turbo Expo: Power for Land, Sea, and Air (Vol. 47276, pp. 553-561).

25.Huang, Y. M., & Liaw, Y. S. (2001). The impact of sliding blades in a rotary compressor. J. Mech. Des., 123(4), 583-589.

26.Simo, J. C., Wriggers, P., Schweizerhof, K. H., & Taylor, R. L. (1986). Finite deformation post-buckling analysis involving inelasticity and contact constraints. International journal for numerical methods in engineering, 23(5), 779-800.

27.Nour-Omid, B., & Wriggers, P. (1986). A two-level iteration method for solution of contact problems. Computer methods in applied mechanics and engineering, 54(2), 131-144.

28.Auricchio, F., & Sacco, E. (1996). AUGMENTED LAGRANGIAN FINITE-ELEMENTS FOR PLATE CONTACT PROBLEMS. International journal for numerical methods in engineering, 39(24), 4141-4158.

29.Tjiu, W., Marnoto, T., Mat, S., Ruslan, M. H., & Sopian, K. (2015). Darrieus vertical axis wind turbine for power generation I: Assessment of Darrieus VAWT configurations. Renewable energy, 75, 50-67.

30.Paraschivoiu, I. (2002). Wind turbine design: with emphasis on Darrieus concept. Presses inter Polytechnique.

31.Clementson, C. L., & Hansen, A. C. (2008). Pilot study of manual sugarcane harvesting using biomechanical analysis. Journal of agricultural safety and health, 14(3), 309-320.

32.Bedon, G., Paulsen, U. S., Madsen, H. A., Belloni, F., Castelli, M. R., & Benini, E. (2017). Computational assessment of the DeepWind aerodynamic performance with different blade and airfoil configurations. Applied Energy, 185, 1100-1108.

388 *33.Abdi, H., & Williams, L. J. (2010). Principal component analysis. Wiley interdisciplinary reviews: computational*
389 *statistics, 2(4), 433-459.*

390 *34.Abdelhafidi, N., Bachari, N. E. I., & Abdelhafidi, Z. (2021). Estimation of solar radiation using stepwise multiple*
391 *linear regression with principal component analysis in Algeria. Meteorology and Atmospheric Physics, 133, 205-*
392 *216.*